Discrete Multiple Material Selective Laser Sintering (M^2SLS): Nozzle Design for Powder Delivery

K. Lappo, K. Wood, D. Bourell, J.J. Beaman
Mechanical Engineering Department
Laboratory for Freeform Fabrication
The University of Texas at Austin, Austin, TX 78712

Abstract

Previous research focused on the advancement of the Selective Laser sintering (SLS) technology to incorporate discrete multiple material processing. The powder delivery subsystem rolled each material sequentially into selectively removed voids in the part bed, produced by vacuum suction, to form a single horizontal layer. This method, although it minimized changes to the traditional SLS technology, produced components with significant material cross contamination between discrete regions. A new powder delivery method was designed to alleviate this problem in which alternatively a nozzle precisely deposits material into vacuum suctioned. Micro-powders, such as those used in SLS, do not readily flow through openings due to the adverse cohesive and drag forces. A uniform powder flow rate for micro-sized particles is achieved by the introduction of pressurized air through the nozzle wall near the outlet. Experiments were performed to determine the optimal hopper back pressure and nozzle injected air pressure to obtain uniform flow rate for the commonly used Duraform PA bulk material.

Introduction

Students at The University of Texas at Austin have pursued Multiple-Material Selective Laser Sintering (M^2SLS) research efforts. M^2SLS is separated into two distinct categories, functionally graded material for FGM (material composition is varied over a distance) and discrete (material regions are separated by discrete boundaries). Perez performed experimental investigations of powder mixing and delivery devices for FGM [1]. WC-Co one dimensional FGM SLS components were built by Jepson [2]. Selective powder delivery methods for M^2SLS were investigated by Jackson and simple discrete M^2SLS components were built using a DTM Sinterstation 2000 [3, 4]. Although simple geometry parts were built successfully using vacuum suction as a selective powder removal method, several process issues arose during the investigation of discrete M^2SLS selective powder delivery subsystems. The focus of this research is to design a powder delivery subsystem for discrete M^2SLS building on previous research results. Design methodology is applied to generate concepts for alternative delivery methods. Figure 1 is a schematic of the material delivery method utilized in preliminary experiments.

Powder Classification

Typically, SLS powders are plastic and polymer coated metal or ceramic in the size range of 40 nm – 150 μm. During processing powder is transported to the build platform by a roller, doctor blade or nozzle. It is necessary to understand the transport behavior of powders in this

size range. Fluidized solids behavior is classified into four groups, characterized by density differences $\left(\rho_s - \rho_f\right)$ and mean particle size [5]. Powders are grouped by broadly similar properties when fluidized by a gas. Behavioral predictions should be limited to individual groups, for many characteristics of fluidized powders are dissimilar even though few are common to all fluidized powders.

Group A consists of materials having a small mean particle size and/or a low particle density (less than 1.4 g/cm^3). Powders in this group are characterized by an appreciable bed expansion before bubbling commences and slow (0.3-0.6 cm/s) collapse upon sudden gas supply cut off. Group B contains powders in the mean size and density ranges 40 μm < d_{sv} < 500 μm and 4 g/cm^3 > ρ_s > 1.4 g/cm^3. In contrast to group A powders, naturally occurring bubbles start to form at or slightly above minimum fluidization velocity. Powders that are cohesive belong in group C. "Normal" fluidization is extremely difficult; the powder lifts as a plug in small diameter tubes or channels (rat-holes) badly. These behaviors are seen because the interparticle forces are greater than those the fluid can exert on the particle. This is generally the result of very small particle size, strong electrostatic charge or high water content. The last classification, group D, is for large and or very dense particles. Figure 1 shows the classification diagram.

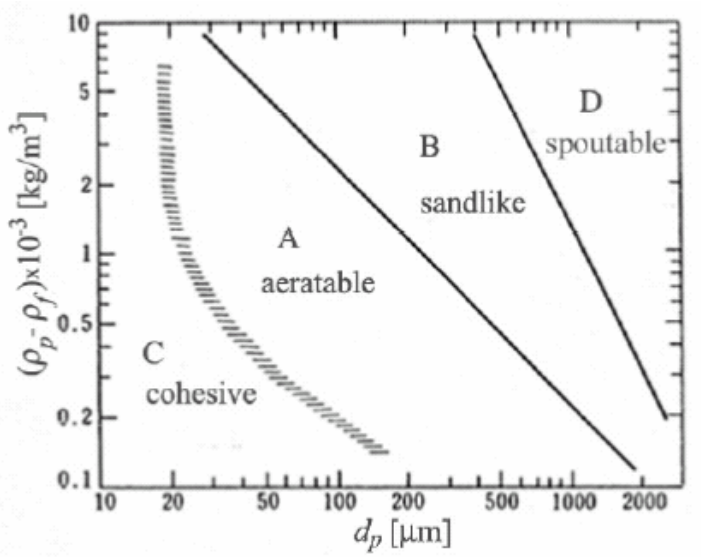

Figure 1: Geldart powder classification diagram for fluidization by air (ambient conditions) [6].

Discrete M^{2}SLS

Building on fundamental knowledge of powder classification discussed above, research focus is turned to a precision powder delivery subsystem. A precision delivery method alleviates process issues encountered with the selective delivery method used in simple geometry part build. A proposed method removes and replaces secondary and possibly primary material roller delivery with nozzle delivery. This will eliminate part shifting and powder cross-contamination issues which arose during preliminary experiments for electrostatic and vacuum powder removal

methods. A schematic of a process where the primary powder is roller delivered and the secondary powder is nozzle delivered is shown in Figure 2.

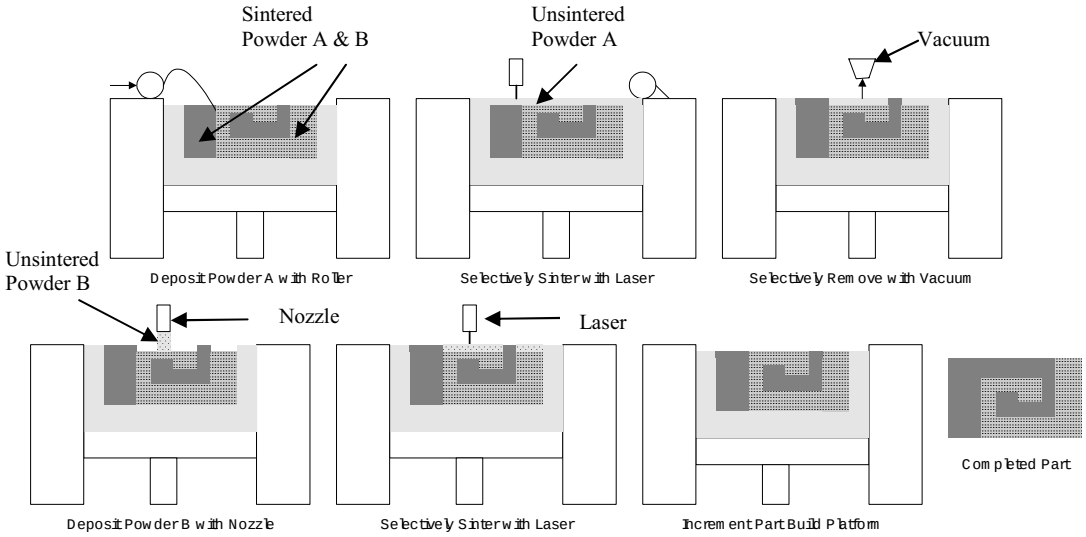

Figure 2: Schematic of precision discrete M^2SLS powder delivery method.

To develop this concept uniform powder delivery must be accomplished. Powder must be taken from storage bins and delivered to the build chamber. The delivery rate, line width and height must be controlled to ensure accurate part geometry. The first step is to investigate the effect of design variables on the rate of powder discharge. A Design of Experiments (DOE) is discussed in the next section.

Nozzle Powder Delivery

A simple nozzle powder delivery experiment is designed to determine the effect of several design variables on the flow rate of two powders, DuraForm PA and CastForm PS. Preliminary trials are performed to determine where control variables will be set for experimentation and bounds for performance variables. Das reports uniform mass flow is achieved for decreased particle size with an increase in back pressure [7]. The delivery back pressure is set at a constant 1.5 psi for experimentation. Nozzle aeration pressures are tested in 0.1 psi increments between 0 psi and 1.0 psi. Trials reveal a high cohesive arching sensitivity to slight decreases in nozzle air pressure. It is found that above 0.1 psi nozzle air pressure tends to disperse the powder turbulently (discharge a large radial spray) or cause cohesive arching after the powder in the nozzle is discharged. Figure 3 displays both the desired and undesired discharge patterns. This second effect is seen when the nozzle pressure exceeded the amount of air required to separate the particles and acts as an upward force on the powder column. Below 0.1 psi the powder intermittently arches cohesively at the beginning of the trial or mid trial. The nozzle aeration pressure is set at 0.1 psi for all trials of the DOE. The design parameters used for the DuraForm PA and CastForm PS experiments are discussed in the next sections.

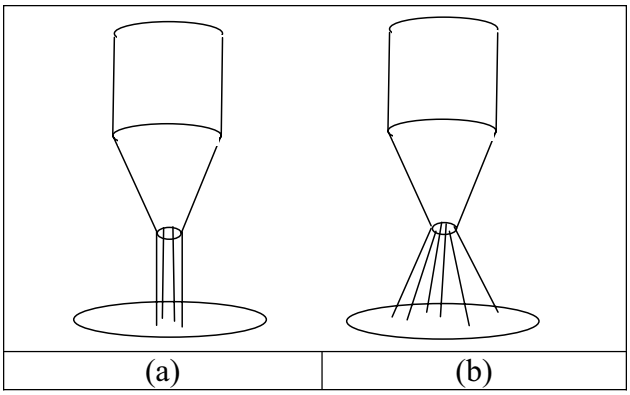

Figure 3: Powder discharge from conical nozzle (a) desired discharge with minimal spray and (b) turbulent discharge with excessive spray.

Nozzle Design

The nozzles were built by traditional SLS out of DuraForm PA. Two sets of four nozzles pictured in Figure 4 were fabricated. The center shaft of one set of nozzles is coated with silver paint which is connected to conductive tape and wired to ground. This allows a pathway for residual charge to travel from the powder. SLS was chosen as the nozzle fabrication method due to the ease of building complex shapes with internal cavities and small channels.

The inner shaft of each nozzle has a 25.0 mm vertical wall with an inlet diameter of 5.0 mm, a half angle of 10.5^{o} and an outlet diameter of 2.5 mm. Each nozzle contains an air inlet and an internal chamber allowing air to pass through the inner wall into the powder pathway. The shape of the nozzle air configuration is varied to determine the effect on powder flow. The spiral configuration is chosen from an analogy design methodology technique and a radial configuration is chosen to investigate a uniform distribution of aeration near the nozzle orifice. A list of the nozzles used in the DOE is given in Table 1.

Nozzle #	Shape	Coating	Standpipe
1	R	N	N
2	S	N	N
3	R	N	Y
4	S	N	Y
5	R	Y	N
6	S	Y	N
7	R	Y	Y
8	S	Y	Y

Table 1: Design nozzles used where R is radial, S is spiral, Y is yes and N is no.

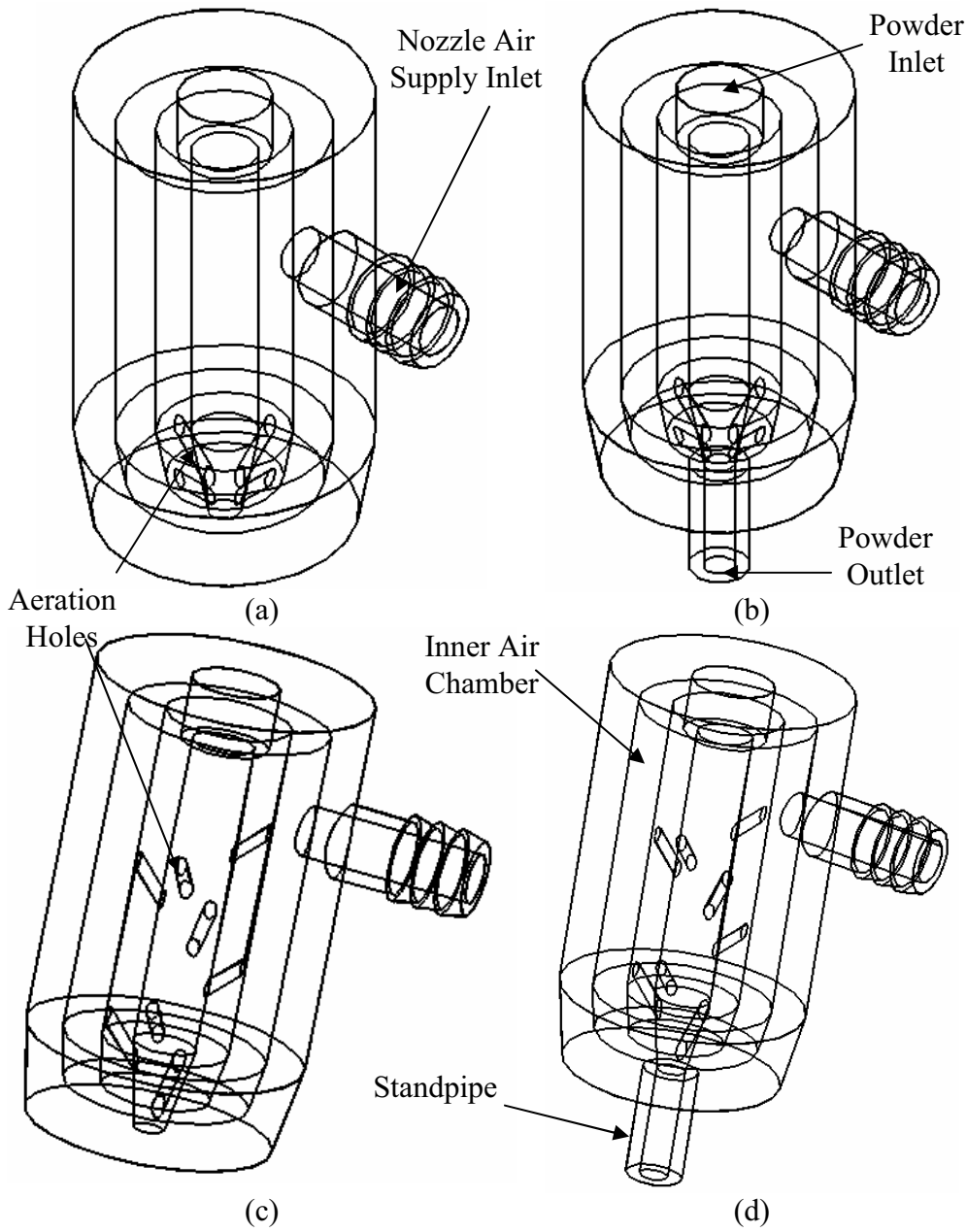

Figure 4: Nozzles used for DuraForm PA and CastForm PS powder delivery DOE (a) radial air configuration, (b) radial air configuration with standpipe, (c) spiral air configuration, and (d) spiral air configuration with standpipe.

Experimental Setup

The mass of powder discharged from interchanged nozzles is measured at timed intervals. Powder is contained in a 52 cm glass tube with a 5.0 mm inner diameter. Individual nozzles are attached to the bottom of the glass tube for the respective trial. A Fisher Scientific A-160 Balance (0.0001 resolution) collects mass measurements at 10 Hz. Two Bellofram regulators (0-5 psi) and Wika pressure gauges (0-3 psi) are used to regulate and monitor the back

and nozzle pressures respectively. Hyperterminal is used to acquire data directly from the balance. Figure 5 is an image of the experimental powder delivery setup.

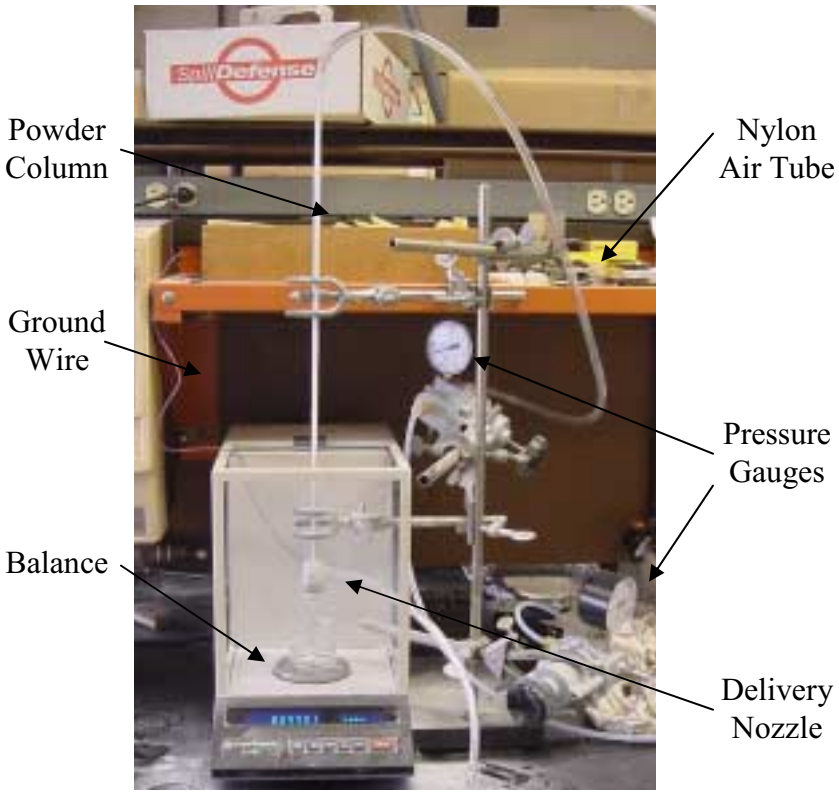

Figure 5: Experimental setup for nozzle powder delivery.

The maximum tube powder capacity is measure before each trial, 4.5 g for DuraForm PA and 4.0 g for CastForm PS. Since a critical height must be maintained for mass flow in a hopper, up to thirteen times the hopper diameter [31], this is critical for data analysis. Pressures are adjusted and the powder is allowed to discharge from the nozzle.

Design of Experiments

A DOE evaluates the individual and coupled effects of design variables on a performance metric [8] of which two are considered, the deviation of mass flow rate from uniform (y_1) and the correlation factor of mass flow rate to a linear trend line (y_2). Both of these metrics are measured as deviations from target values where the targets. Uniform flow is represented by a zero slope mass flow rate curve with a correlation factor of one. The number of trials (N) is set at 2^n, where n is the number of design variables. The number of experiments performed (X) is double the number of trials and they are randomized to prevent in accuracy due to noise. Separate experiments are performed for two materials, DuraForm PA and CastForm PS. Discharge of powder is seen with all nozzle geometry variations for DuraForm PA but not for CastForm PS, therefore the design variables are not the same. During initial investigation of CastForm PS delivery, initial and intermittent cohesive arching is encountered with nozzles with a standpipe,

therefore the nozzles containing a standpipe are remove from the experiment. Experimental design variables for both experiments are given in Tables 2 and 3.

d_1 : Air Inlet Shape	d_2 : Coating (Silver Paint)	d_3 : Standpipe
+	4 x radial	Yes	Yes
-	8 x helix	No	No

Table 2: Design variables for DuraForm PA delivery experiment.

d_1 : Air Inlet Shape	d_2 : Coating (Silver Paint)
+	4 x radial	Yes
-	8 x helix	No

Table 3: Design variables for CastForm PS nozzle powder delivery experiment.

In addition to both control and design variables, noise variables must be taken into account. Several test conditions contribute to inconsistent mass flow patterns and tendencies toward cohesive arching. Environmental humidity can have an effect of powder behavior due to polymer susceptibility to water absorption. Also, the test temperatures for these experiments are well below the build temperature, 180^{o} C and 86^{o} C for DuraForm PA and CastForm PS respectively. Interparticle and particle-wall friction contribute to uniform flow resistance. SLS parts, regardless of the material system used, present a grainy surface finish due to the powder particle size, the layer-wise building sequence and to the vibration of the roller mechanisms during powder delivery [9]. Extensive noise can cause performance metric sensitivity to design variables to be statistically insignificant if prominent.

Collected Data

The mass flow rate is derived from the interval mass measurements and the measurement rate. Both the cumulative mass and flow rate are plotted. Figure 6 is a plot representative of the data collected during most trials. This plot is data from DuraForm PA experiment nine (trial 3) corresponding to a radial aeration configuration, no conductive inner wall coating and a standpipe. The flow rate starts off fairly uniform and increases as the powder level reaches the critical height required to maintain mass flow. As the remaining powder is pushed from the glass tube there is a sharp peak in the mass due to the force on the balance due to the back and nozzle air flows and a recoil as the air pressure is relieved. Performance metric analysis is performed on mass measurements before the critical height is reached.

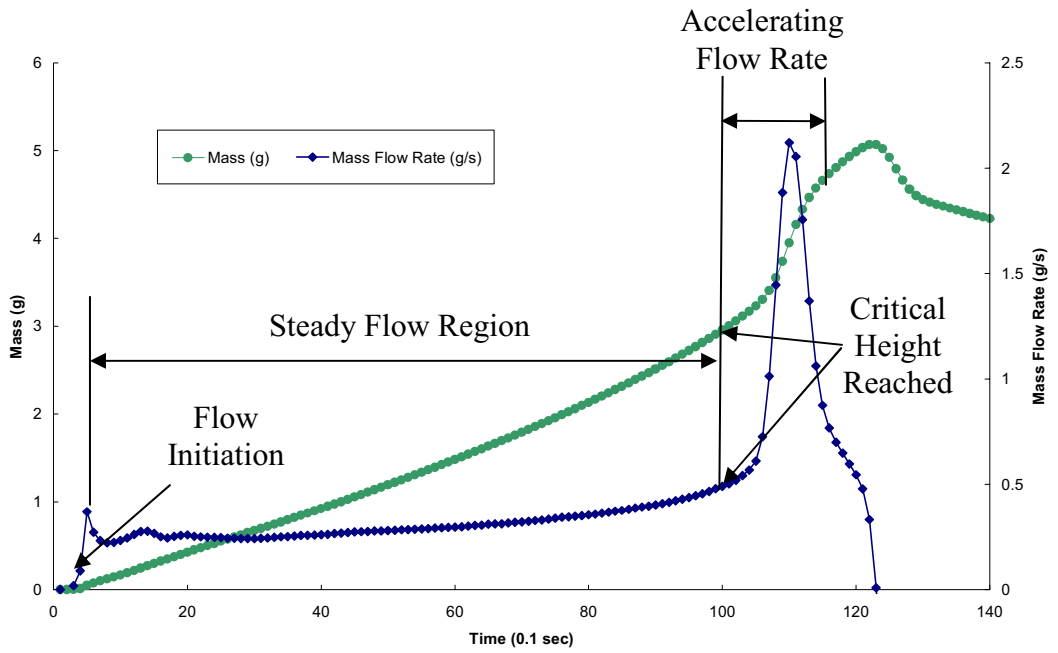

Figure 6: DuraForm PA experiment 9 trial 3 data plot (radial air configuration, no conductive coating and with standpipe).

The effect of change in design variables on powder flow in the steady flow region of the data plot is of interest. The mass flow curve from the flow initiation point to the critical height point is fit to a linear curve. The mass flow rate uniformity is measured as the absolute value of the deviation in the slope of the curve from zero, which is represented in Equation 5.1. The correlation factor is calculated as the least squared sum of a linear trend line deviated from one.

$$y_1 = \left| 0 - \dot{m} \right| \quad (1)$$

Sixteen experiments, two replicates (r) of eight trials, are performed for the DuraForm PA DOE. The data is represented in two matrices (each with size X by 1) for the uniformity of mass flow rate and correlation factor measurements respectively. The normalized values for DuraForm PA design variable and coupled term high and low bounds are represented by "1" and "-1", presented in Tables 4. Similarly, eight experiments are performed for CastForm PS powder delivery investigation. Table 5 represents the collected data from this DOE.

Experiment	Trial #	Mean	d1	d2	d3	d1d2	d1d3	d2d3	d1d2d3	y1	y2
2	8	1	-1	-1	-1	1	1	1	-1	0.5639	0.0374
5	8	1	-1	-1	-1	1	1	1	-1	0.2674	0.0135
1	7	1	-1	-1	1	1	-1	-1	1	0.0215	0.8800
13	7	1	-1	-1	1	1	-1	-1	1	0.0690	0.6030
4	6	1	-1	1	-1	-1	1	-1	1	0.0416	0.4680
16	6	1	-1	1	-1	-1	1	-1	1	0.2790	0.1929
11	5	1	-1	1	1	-1	-1	1	-1	0.1420	0.1318
14	5	1	-1	1	1	-1	-1	1	-1	0.1170	0.1949
3	4	1	1	-1	-1	-1	-1	1	1	0.0237	0.0420
7	4	1	1	-1	-1	-1	-1	1	1	0.0460	0.0216
9	3	1	1	-1	1	-1	1	-1	-1	0.0210	0.2311
12	3	1	1	-1	1	-1	1	-1	-1	0.0210	0.3823
10	2	1	1	1	-1	1	-1	-1	-1	0.0270	0.0910
15	2	1	1	1	-1	1	-1	-1	-1	0.0900	0.1713
6	1	1	1	1	1	1	1	1	1	0.0210	0.1932
8	1	1	1	1	1	1	1	1	1	0.0260	0.0812

Table 4: Collected data from DuraForm PA DOE.

Exp #	Trial #	Mean	d1	d2	d1d2	y1	y2
1	4	1	-1	-1	1	0.0229	0.1061
4	4	1	-1	-1	1	0.0095	0.1081
5	3	1	-1	1	-1	0.0199	0.1174
6	3	1	-1	1	-1	0.0019	0.3880
2	2	1	1	-1	-1	0.0015	0.3492
7	2	1	1	-1	-1	0.0015	0.3258
3	1	1	1	1	1	0.0011	0.3047
8	1	1	1	1	1	0.0021	0.2052

Table 5: Collected data from CastForm PS DOE.

Results and Discussion

Nozzle powder delivery of DuraForm PA and CastForm PS shows promise due to the majority of data collected that show seemingly uniform mass flow rates with little pulsing. Three trials between both DOEs resulted in repeatable results for both y_1 and y_2 for repeat experiments. The powder flow behavior is consistent and the total powder discharge time for replicate experiments in all cases is +/- 0.5 sec. Figures 7 and 8 are data plots of mass flow rate for the DuraForm PA and CastForm PS repeatable trial results. In addition to these promising results, several trials resulted in repeatability of either y_1 or y_2 but not both. These plots are presented in the Appendix with the full set of plots and data tables.

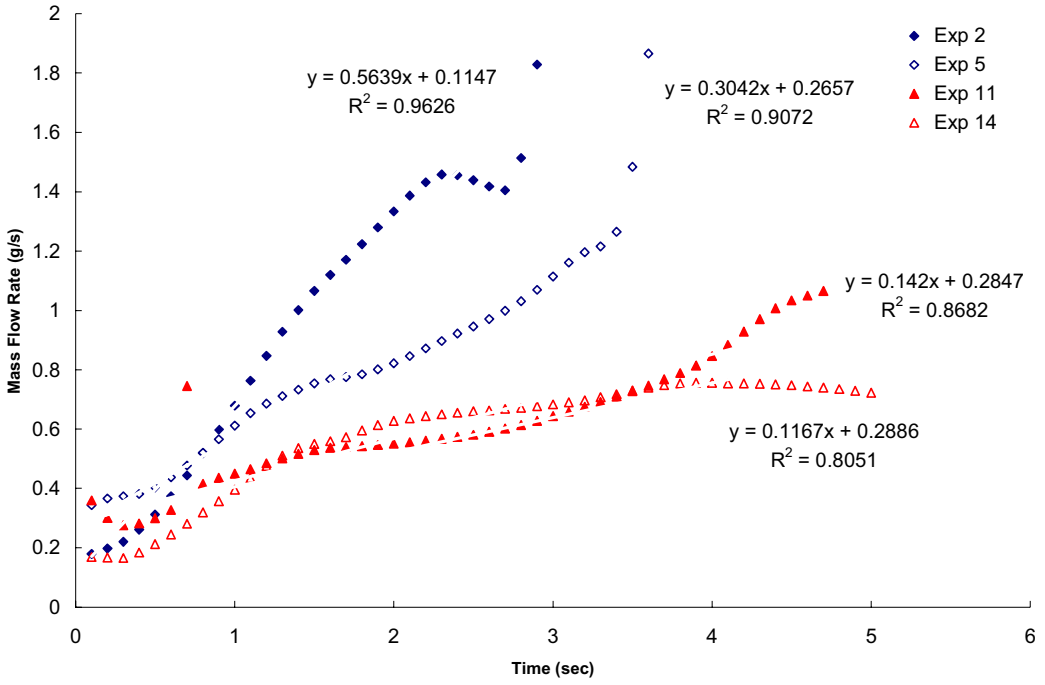

Figure 7: Repeatable trial results from DuraForm PA DOE for both y_1 and y_2, experiments 2 and 5 from trial 8 and experiments 11 and 14 from trial 5.

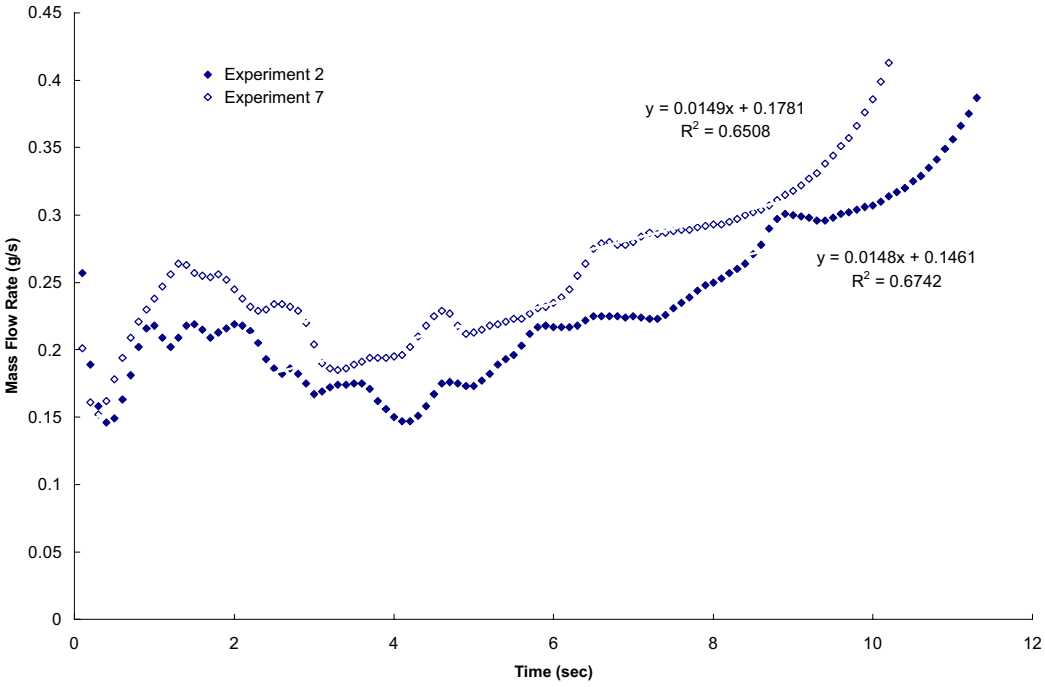

Figure 8: Repeatable trial results from CastForm PS DOE for both y_1 and y_2, experiments 2 and 7 from trial 2.

Unfortunately, results were not consistent during testing due to excessive noise. For example, only one data set was collected for attempts with all nozzle geometries with no nozzle

aeration pressure, shown in Figure 9. Fortunately, this plot shows a fairly uniform mass flow rate with an average powder acceleration of 0.0011 g/s^2 and minimal deviation from this trend line near the onset of discharge. This result shows promise for the investigation of nozzle parameters not studied in these experiments in coordination with aeration configuration. Replicate data sets with these parameters were unable to be collected due to cohesive arching.

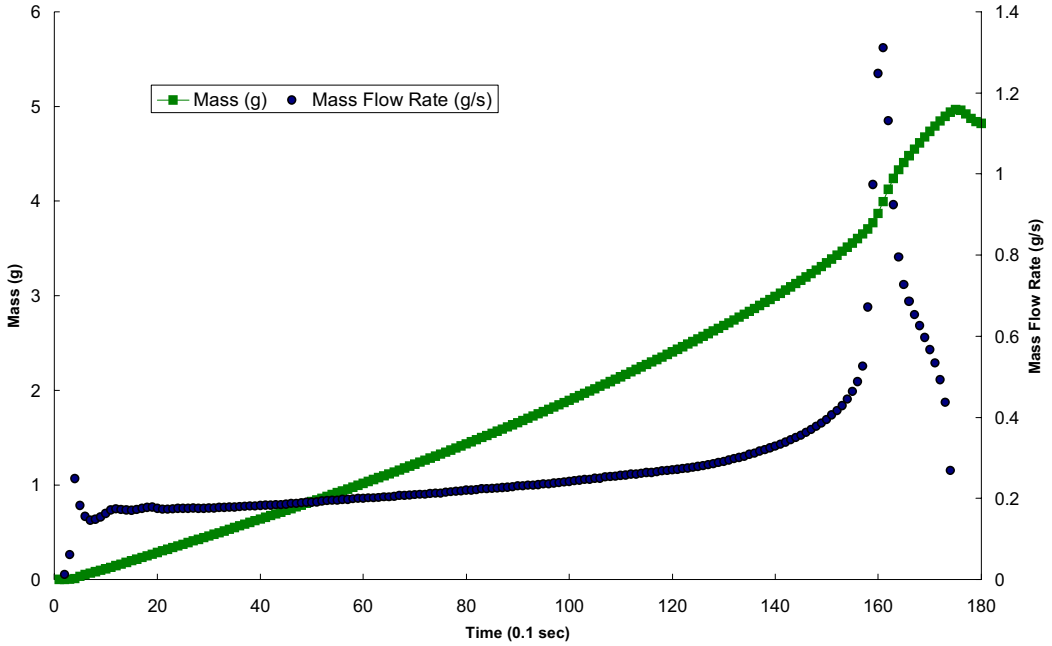

Figure 9: DuraForm PA powder delivery with no nozzle aeration pressure, radial aeration configuration, no conductive inner wall coating and no standpipe.

A trend observed in the mass flow rate of a few data sets is a linear increase to a uniform rate before reaching the critical powder height. Figure 10 is from DuraForm PA experiment 15 (trial 2) corresponding to a radial aeration configuration with a conductive coating and no standpipe. A significant deviation from zero slope and correlation factor of one is seen in these plots of mass flow rate. This flow behavior is not duplicated in the replicate experiment of trial 2, which caused significant noise in the data set.

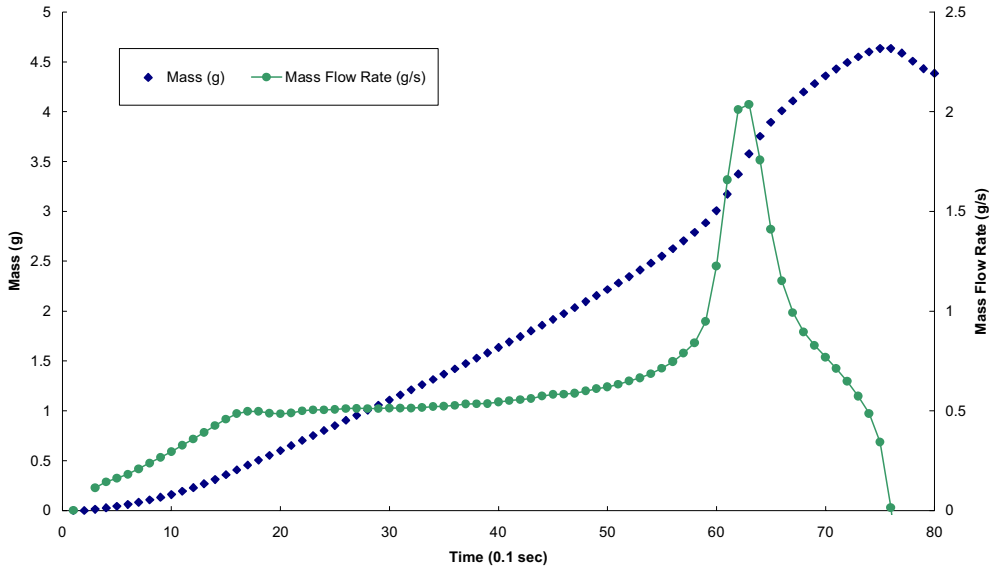

Figure 10: DuraForm PA experiment 15 (trial 2) corresponding to a radial aeration configuration with a conductive coating and no standpipe.

Inconsistent flow is seen in two DuraForm PA experiments. The powder in the glass tube does not steadily fall into the nozzle, but the nozzle aeration steadily clears the pathway. An unsteady mass flow rate is observed in these instances as shown in Figure 5.10 representing data from experiment one (trial 7) having a spiral aeration configuration and a conductive wall coating but no standpipe. The mass flow rate of this experiment is clearly not uniform. The resulting correlation factor is the minimum seen for all experiments at 0.12 with a deviation from 1.0 of 0.82. These two plots significantly contributed to the noise in the DuraForm PA DOE.

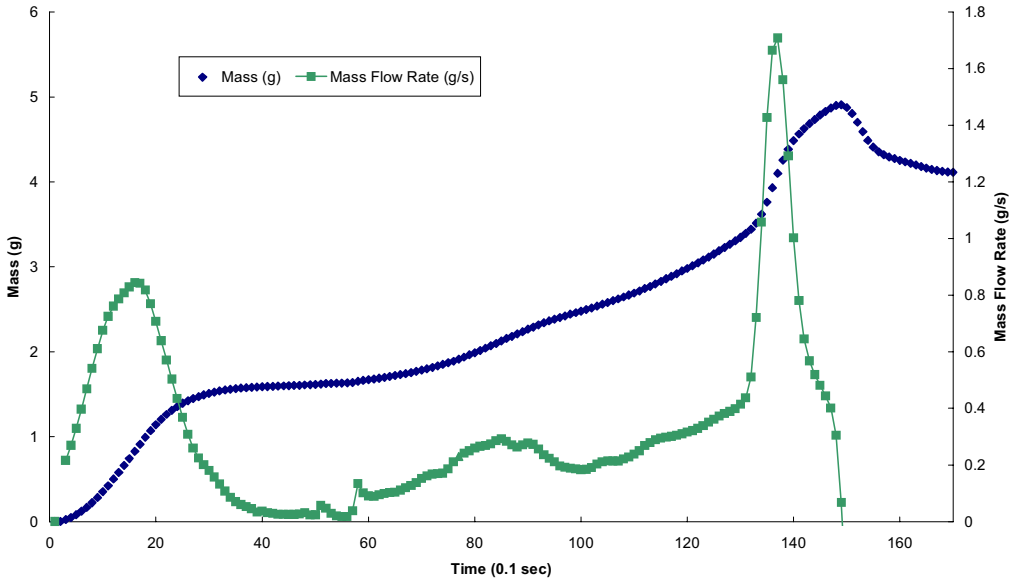

Figure 11: DuraForm PA experiment one (trial 7) having a spiral aeration configuration and a conductive wall coating but no standpipe.

Analysis of Variance (ANOVA)

ANOVA is used to test the significance of performance metric sensitivity to individual design variables and couples effects. These research efforts focused on two performance metrics of deviation of mass flow rate from uniform and flow rate data correlation factor as discussed above. The collected data is utilized to form two matrices, [X] and [y]. The [X] matrix is comprised of the mean, individual and coupled normalized terms, having the same number of rows as experiments performed and the same number of columns as trials. The [y] matrix is a column vector with the number of rows equal to the number of experiments performed. The sensitivity coefficients are found using the matrix operation of Equation 2, which form the general formulas for two and three variable linear models given in Equations 3 and 4 respectively:

$$[\beta] = \left([\mathrm{X}]^T [\mathrm{X}]\right)^{-1} [\mathrm{X}]^T [y] \quad (2)$$

$$P = \beta_0 + \beta_1 d_1 + \beta_2 d_2 + \beta_{12} d_1 d_2 + error \quad (3)$$

$$P = \beta_0 + \beta_1 d_1 + \beta_2 d_2 + \beta_3 d_3 + \beta_{12} d_1 d_2 + \beta_{13} d_1 d_3 + \beta_{23} d_2 d_3 + \beta_{123} d_1 d_2 d_3 + error \quad (4)$$

The probability of significance of each sensitivity coefficient is determined using ANOVA. The terms associated with coefficients deemed significant with a 90% confidence remain in the model. Other terms are considered to be part of the noise and are dropped from the model equation.

Another method for determining statistical noise is to calculate the standard deviation (σ) of [y] data. The statistical noise is considered to be three times the standard deviation. If a sensitivity factor, $E = 2\beta$, is less than the statistical noise, it can be considered insignificant to the performance.

DuraForm PA

Collected data in Table 4 is used to calculate the performance metric sensitivity coefficients for the DuraForm PA DOE. The statistical noise is 0.0185 and 0.2660 for the y_1 and y_2 data respectively. Performance metric sensitivity coefficients for both sets of DuraForm PA data are summarized in Table 6. Only the sensitivity coefficient β_0 is significant in comparison to the statistical noise for y_1. Two coefficients are significant in the correlation factor data, β_0 and β_{23}. ANOVA is performed to compare statistical significance confidence using the F-test.

Trial	Mean	d_1	d_2	d_3	d_1d_2	d_1d_3	d_2d_3	$d_1d_2d_3$
$Beta_1$	**0.0111**	-0.0077	-0.0018	-0.0056	0.0025	0.0044	0.0040	-0.0045
$Beta_2$	**0.2333**	-0.0816	-0.0427	0.1039	0.0252	-0.0337	**-0.1442**	0.077

Table 6: Average powder acceleration DuraForm PA experimental results.

No sensitivity coefficients are significant within a 90% confidence using ANOVA for the average powder acceleration data. The coefficients β_1 and β_{12} have the highest level of confidence. β_1 corresponds to the individual performance sensitivity to aeration configuration in the nozzle. The notably higher significance to change in performance metric shows a stronger

effect on aeration configuration as a design variable. All coupled coefficients have confidence levels <90% for the y_2 data set, which only compares with the β_{23} significance from earlier findings. These values are highlighted in Table 7.

Term	Variable	DOF	SS_1	SS_2	MS_1	MS_2	$F0_1$	$F0_2$	P_1	P_2
B0	mean	1	0.0326	0.1084	0.0326	0.1084	1.00	1.00	0.65	0.65
B1	d1	1	0.0939	0.1069	0.0939	0.1069	2.88	0.99	0.87	0.65
B2	d2	1	0.0053	0.0295	0.0053	0.0295	0.16	0.27	0.30	0.38
B3	d3	1	0.0506	0.1722	0.0506	0.1722	1.55	1.59	0.75	0.76
B12	d1d2	1	-0.0774	-0.3481	0.0774	0.3481	2.37	3.21	0.84	0.89
B13	d1d3	1	-0.0082	-0.8274	0.0082	0.8274	0.25	7.63	0.37	0.98
B23	d2d3	1	-0.0269	-0.9800	0.0269	0.9800	0.83	9.04	0.61	0.98
B123	d1d2d3	1	-0.0613	1.0139	0.0613	1.0139	1.88	9.35	0.79	0.98
Total	n/a	15	0.3243	0.8625	0.0216	0.0575				
Error	n/a	8	0.2608	0.8673	0.0326	0.1084				

Table 7: ANOVA results for DuraForm PA delivery data.

The slopes and correlation factors analyzed are on a small scale (0 – 1). Deviation in a sample causes a large standard deviation in the set. It is consistent that the statistical analysis reveals sensitivity factors to have low confidence levels. The average deviation from uniform mass flow rate slope is 0.0111 g/s^2 for the DuraForm PA experiments with a low of 0.0021 g/s^2 and high of 0.0564 g/s^2.

CastForm PS

Similar results are seen in the CastForm PS data. Table 8 lists the sensitivity coefficients for the y_1 and y_2 performance metrics respectively. The statistical noise for these data sets are 0.0172 and 0.2098. Comparing these coefficients to the noise, only the mean sensitivity coefficient for the deviation from uniform flow rate data is greater than the noise. ANOVA is used to test if any coefficients have significance with confidence <90%.

Trial	Mean	d_1	d_2	d_1d_2
$Beta_1$	**0.0075**	-0.006	-0.0013	0.0013
$Beta_2$	**0.2381**	0.0582	0.0158	-0.057

Table 8: Average powder acceleration CastForm PS experimental results.

As seen with DuraForm PA, no coefficients reach a 90% confidence significance level. The β_1 and β_{12} coefficients have the highest level of confidence as seen in the DuraForm PA data. DuraForm PA and CastForm PS have similar material properties and particle size distributions. The average particle diameters are 58 μm and 62 μm for DuraForm PA and CastForm PS respectively with particle size range of 25-106 μm [10-11]. The densities of the two powders are also comparable at 0.97 g/cm^3 and 0.86 g/cm^3 (ASTM D792). The ANOVA for the deviation from uniform mass flow rate showed no significant coefficients also.

Term	Variable	DOF	SS_1	SS_2	MS_1	MS_2	$F0_1$	$F0_2$	P_1	P_2
B0	mean	1	0.0001	0.0688	0.0001	0.0688	1.00	1.00	0.63	0.63
B1	d1	1	0.0003	0.0271	0.0003	0.0271	2.25	0.39	0.79	0.44
B2	d2	1	0.0000	0.0020	0.0000	0.0020	0.11	0.03	0.24	0.13
B12	d1d2	1	-0.0002	-0.3295	0.0002	0.3295	1.78	4.79	0.75	0.91
Total	n/a	7	0.0006	0.0969	0.0001	0.0138				
Error	n/a	4	0.0005	0.2752	0.0001	0.0688				

Table 9: ANOVA for average powder acceleration CastForm PS results.

The presence of desired data trends shows promise in powder delivery by nozzle with aeration through the wall. Further investigation of alternative design parameters such as nozzle material (wall friction coefficient), half angle, inlet diameter, outlet diameter and nozzle shape in coordination with the design variables evaluated in these DOEs will aid in understanding powder behavior. Several factors are considered for improvement of powder delivery by nozzles.

Two materials were investigated in this research effort, which are readily available, but very similar in size, distribution and properties. The goal of powder delivery for multiple materials is to have the ability to deliver any material desired dependent on application. DuraForm PA and CastForm PS are two polymer powders currently used commercially with small particle sizes (25-106 μm). These materials were chosen because delivery of smaller powders is difficult. Cohesive attraction between particles causes unpredictable powder behavior. Experimental improvements will be seen when a broad base of materials are investigated.

DuraForm PA nozzles built with traditional SLS, which proved to be a large source of statistical noise. The surface roughness of SLS parts is typically in the range of the bulk powder size. Powder delivery through a nozzle is complicated by additional friction factors. The wall friction contributes to undesired flow behavior. The use of a polymer contributes to the build up of residual electrostatic charge along the wall and powder. The use of an alternative nozzle material for powder delivery will reduce the noise due to particle-wall interaction. A polished inner channel wall will reduce friction and a grounded metallic nozzle material will provide a pathway for charge removal.

Experimental environmental conditions for data collection are far from normal operating conditions for DuraForm PA and CastForm PS. Both powders are processed at elevated temperatures, in excess of 80^{o}C, and additional environmental controls. These experiments were performed at room temperature with no humidity control or monitoring. Additional equipment would be required to provide these parameters. Nozzle powder delivery will be more accurate when investigation is performed as close to realistic operating conditions as possible.

One nozzle geometry and two aeration configurations were investigated in these experiments. The aeration holes are 1.0 mm diameter (smallest SLS feature size), which should be reduced for optimal performance. Both the nozzle geometry parameters; diameters, half angle and shape and aeration configuration should be varied to determine the optimal performance for powder delivery of a given material. A simple radial arrangement with four holes was used, where the number of holes could be varied along with the placement of the holes. A straight vertical line could be used similar to the spiral configuration.

A 52 cm glass tube was used as the powder hopper for powder discharge. The amount of data observed to have a relatively uniform mass flow rate comprises a small fraction of the column height. The use of a larger powder column will allow the collection of larger data sets per experiment. In addition, the implementation of controls in the future to eliminate any fluctuation in back and nozzle pressures will prevent the fluctuation of mass flow rate from uniformity.

There is promise for delivery of powder with nozzles. Success was observed with other gravity powder discharge experiments at The University of Michigan [7]. Positive data was observed in these research efforts. With the incorporation of the noted improvements discrete multiple material powder delivery has the potential of success.

References

[1] Perez, J. (1999). *Powder Delivery for a Multiple Material Selective Laser Sintering Machine*, Masters Thesis, University of Texas at Austin.

[2] Jepson, L. (2002). Multiple Material Selective Laser Sintering, PhD Dissertation, University of Texas as Austin.

[3] Jackson, B., Wood, K., Beaman, J. (2000). "Discrete Multi-Material Selective Laser Sintering (M^2SLS): Development for an Application in Complex Sand Casting Core Arrays", *Proceedings of the Solid Freeform Fabrication Symposium*, University of Texas at Austin, pp 176-182.

[4] K. Lappo, B. Jackson, K. Wood, D. Bourell, J.J. Beaman (2003). "Discrete Multiple Material Selective Laser Sintering (M^2SLS): Experimental Study of Part Processing," *Proceedings of the Solid Freeform Fabrication Symposium*, University of Texas at Austin, submitted.

[5] Geldart, D. "Types of Gas Fluidization", Powder Technology, 7 (1973) 285-292.

[6] Kobayashi, T., Kawaguchi, T., Tanaka, T. and Tsuji, Y., "DEM Analysis on Flow Patterns of Geldart's Group A Particles in Fluidized Bed," Proc. of World Congress on Particle Technology 4 (CD-ROM), July 21-25, Sydney, Australia, (2002), Paper No. 178.

[7] Santosa, J. "Expterimental and Numerical Study on the Flow of Fine Powders from Small-scale Hoppers Applied to SLS Multi-Material Deposition", Proceedings of the Solid Freeform Fabrication Symposium, 2002, pp 620-627.

[8] Otto, K., Wood, K. (2001). Product Design: Techniques in Reverse Engineering and New Product Development, Prentice Hall, NJ.

[9] I.Y. Tumer; D.C.Thompson, K.L.Wood and R.H. Crawford, "Characterization of Surface Fault Patterns with Application to a Layered Manufacturing Process", Journal of Manufacturing Systems, Vol. 17, No.1, 1998.

[10] DTM Corporation (1997). "The Sinterstation® System Guide to Materials: DuraForm™ Polyamide," Dec 1997, DCN: 8001-10014.

[11] DTM Corporation (1999). "The Sinterstation® System Guide to Materials: CastForm Polystyrene," April 1999, DCN: 8002-10006.